



Preparation of activated carbon from pine (*Pinus radiata*) sawdust by chemical activation with zinc chloride for wood dye adsorption

Catarina H. Pimentel¹ · M. Sonia Freire¹ · Diego Gómez-Díaz¹ · Julia González-Álvarez¹

Received: 29 December 2022 / Revised: 14 March 2023 / Accepted: 24 March 2023
© The Author(s) 2023

Abstract

Wastewater containing dyes are released into water bodies generating serious problems in human health and marine life. To contribute to the solution of this problem, a novel activated carbon was prepared from untreated pine (*Pinus radiata*) sawdust by dry chemical activation with ZnCl_2 and was used for wood dye adsorption. The carbon was characterized by point of zero charge, N_2 and CO_2 adsorption isotherms, SEM-EDX, and FTIR. N_2 and CO_2 surface areas were 471.4 and 319.5 $\text{m}^2 \text{g}^{-1}$, respectively, with 91% of micropores. Wood dye adsorption was studied in function of pH (2–12), adsorbent dose (0.1–4 g L^{-1}), time (up to 48 h for blue and red and 12 h for black), and initial concentration (5–500 mg L^{-1}). The equilibrium data for the blue and black dyes were satisfactorily fitted to the Freundlich model while those for the red dye to the Langmuir model. Kinetic data were explained by the pseudo-second order (chemisorption process) and intraparticle diffusion models. At 5 mg L^{-1} , a 100% removal efficiency was achieved at all pH for the blue dye, whereas for the red and black, natural pH (5.1) and pH = 2, respectively, led to the best removal efficiencies, 96 and 56%. Increasing concentration above 25 mg L^{-1} significantly reduced adsorption efficiency for blue and red dyes. For the black dye increasing the dose to 1 g L^{-1} , the adsorption efficiency reached 82% at 25 mg L^{-1} . High removal efficiencies were achieved for all dyes at 25 mg L^{-1} and 4 g L^{-1} .

Keywords Activated carbon · Chemical activation · Zinc chloride · Adsorption · Pine sawdust · Wood dyes

1 Introduction

A problem that has persisted over the years and has attracted the attention of many researchers is water pollution. With the huge expansion of industrialization (such as textile, wood, rubber, and dye industries), the volume of untreated wastewaters that are discharged into streams and water bodies also increased. Among the wastewater contaminants, particularly dyes can generate serious problems in human health due to their toxicity, mutagenicity, and carcinogenicity even at low concentrations. Moreover, they are highly resistant to light, aerobic digestion, and oxidizing agents due to their chemical stability [1–3]. Therefore, wastewater treatment is essential and various technologies have been employed for dye removal such as electrocoagulation; photocatalytic, oxidative, and biochemical degradation; and adsorption.

Adsorption has received special attention due to its simplicity, high efficiency, including the treatment of concentrated dye effluents, low cost, and the possibility of reusing the adsorbent through its recovery and regeneration [4, 5].

Adsorption on activated carbons (AC) has been widely used for dye removal due to their high porosity, surface area, physicochemical stability, mechanical strength, and surface reactivity. However, due to their high cost and regeneration difficulty, numerous investigations have focused on their production from natural, abundant, safe, and low-cost precursors [6–8]. Activated carbons can be prepared by physical (in which steam, nitrogen, or carbon dioxide can be used for moderate reduction of the carbonaceous matter) or chemical activation (a chemical dehydrating agent is employed to activate the biomass or char) by one- or two-step processes. Usually, activated carbon prepared by chemical activation presents higher surface area, smaller pore size, and has wider use in many applications [9, 10]. Agarwal et al. [4] reported the two-step process as the most effective due to the high porosity developed: (1) carbonization of the material under an inert atmosphere which enables the removal of moisture, volatile compounds, and other aromatic and then resulting

✉ Julia González-Álvarez
julia.gonzalez@usc.es

¹ Department of Chemical Engineering, School of Engineering, Universidade de Santiago de Compostela, 15782 Santiago de Compostela, Spain

in a char with high carbon content; and (2) activation at elevated temperature to degrade the cellulosic materials in the precursor and to attain specific characteristics which will depend on the process conditions used. Carbonization depends on several factors such as the existence of an inert atmosphere, the heating rate, the carbonization temperature, and time [5, 10]. The resulting char can be activated through chemical activation that could be performed by impregnation (wet oxidation) or by mixing the char with the solid activating agent (dry oxidation) [11–13]. Regarding the activating agents, they act as dehydrating agents which influence the decomposition by pyrolysis and inhibit the formation of tar. Additionally, the activation agent will strongly influence the properties of the activated carbon. Among the most used activating chemical agents such as ZnCl_2 , KOH , H_3PO_4 , and K_2CO_3 , which present an enhanced effect on carbon surface area and porosity, ZnCl_2 stands out as an excellent activating agent [4]. The activation process using ZnCl_2 increases the yield due to polymerization and operates as a Lewis acid favoring the creation of certain large-ring aromatic compounds, produces a template effect inducing the formation of uniform micropores and could be more selective [3, 11, 14, 15]. Moreover, the carbon activated with this agent usually presents outstanding properties such as large pore volume with smaller pore size, higher surface area, and abundant reactive groups for contaminant uptake. Additionally, it has been reported that activated carbons prepared using ZnCl_2 as activating agent showed good results particularly for dye removal [16, 17]. Activated carbon, as general adsorbent, has a long history of manufacture and application, although there are still various production aspects that could be considerably improved [18].

Waste biomass from agricultural or forest byproducts has arisen as the best alternative since these raw materials can be used as adsorbents without treatment, or by carbonization and activation, improving their adsorption capacity. Besides, unwanted and abundant wastes can be converted into useful and valuable adsorbents [19]. There has been demand for cost-effective precursors for the production of activated carbon and recent research have reported the preparation of AC from materials such as grape stalk, semi-coke, coconut shell, slash pinewood, and *Sterculia alata* nutshell [5, 9, 14, 19, 20]. This type of carbon-based materials demonstrates characteristics such as high surface area, stability, range of functional groups, and a porous structure [5]. Nevertheless, depending on the nature of the biomass and the pyrolysis/activation conditions, biochar with a porous structure and different carbon content having a high surface area can be produced [21]. Both chemical structure and surface chemistry depend not only on the type of biomass but also on the parts of the biomass. Cellulosic biomass usually consists of cellulose, hemicelluloses, and lignin but the proportions change depending on the material which will influence the characteristics of activated carbons

[22, 23]. Furthermore, in most of the studies [5, 14, 19, 20], the raw material is washed or pre-treated which increases the use of chemicals in the production of activated carbon. Different waste biomass has been converted into activated carbon and has been successfully used to remove acid dyes from wastewaters: *Paulownia tomentosa* wood to remove acid red 4 [24], apple wood to remove acid red 337 and acid blue 349 [25], walnut and poplar woods to remove acid red 18 [26], pine-cone to remove acid black 1 and acid blue 113 [27].

Pine trees of different species are present in large amounts around the world and are among the most commercially valuable tree species for timber or wood pulp [28]. Pine sawdust, a byproduct from the wood industry, is a lignocellulosic material containing hemicellulose, cellulose, lignin, and some functional groups (e.g., carboxyl, phenolic, hydroxyl) which makes it a good precursor to produce activated carbons [6]. Pine sawdust from *Pinus radiata*, an abundant species in the northwest of Spain, could be an exceptional choice from an economic and environmental viewpoint due to its availability and low cost. To the best of our knowledge, pine sawdust from *Pinus radiata* has never been applied as raw material for the production of activated carbon for dye adsorption [28, 29].

Due to the great concern with the discharge of wastewater containing dyes into water bodies that pose a diversity of hazards for humans and marine life, the present study was focused on the production and characterization of a novel activated carbon based on untreated pine (*Pinus radiata*) sawdust (PS). The carbon was activated by direct mixing with ZnCl_2 and used for the removal of acid wood dyes from aqueous solutions. Thus, a double objective is achieved, to replace expensive commercial activated carbons and at the same time reduce the costs of biomass waste management, in addition to proposing an alternative for solving the challenge of dye wastewater pollution. Batch adsorption experiments were performed to evaluate the influence of various operating conditions such as pH, adsorbent dose, and initial dye concentration on the removal efficiency. The carbon was characterized for its structural and surface properties, by the point of zero charge (pH_{PZC}), BET surface area obtained from nitrogen (N_2) and carbon dioxide (CO_2) sorption isotherms, and pore volume. Also, Fourier transform infrared spectroscopy (FTIR) and scanning electron microscopy coupled with energy dispersive X-ray analysis (SEM-EDX) were performed before and after adsorption. Kinetic and equilibrium studies were carried out under selected conditions in order to analyze the adsorption mechanism.

2 Experimental section

2.1 Materials

Pine (*Pinus radiata*) sawdust (PS) was provided by a regional sawmill (Lugo, Spain). After air-drying to

equilibrium moisture content (11.61 wt%), PS was sieved and the fraction between 0.5 and 1 mm was selected, stored in a plastic container, and used directly for the AC production.

Acid wood dyes were used: Blue for wood AGN-270%, Red for wood GRA-200%, and Black Hispalan M-RN-140%. Dye solutions were prepared by dilution of a stock aqueous solution of 1000 mg L⁻¹ with distilled water. Natural pH was determined for each dye at 5, 25, and 500 mg L⁻¹ using a digital pH meter (Hanna edge).

Zinc chloride (ZnCl₂, 98%, Scharlau), sodium chloride (NaCl, 99.5%, Probus), sodium hydroxide (NaOH, 98%, Sigma-Aldrich), and hydrochloric acid (HCl, 37%, Sigma-Aldrich) were used.

2.2 Production of activated carbon

To analyze the transformations of pine sawdust during the thermal treatment, thermogravimetric analysis was performed from 50 to 1000°C under N₂ atmosphere at 25 mL min⁻¹. According to the results (Fig. S1), 600°C was selected as carbonization temperature since cellulose, hemicelluloses, and lignin decomposition usually takes place below this temperature [15, 30] and no weight loss occurred at higher temperatures.

PS was carbonized at 600°C for 1 h under a N₂ atmosphere (10 mL min⁻¹) in a horizontal tubular furnace (Carbolite, Sheffield) applying a ramp of 5°C min⁻¹ up to 600°C. Afterward, it was cooled down to room temperature. Thereafter, the biochar produced after carbonization was mixed by milling with ZnCl₂ at a weight ratio of 1:4 (w/w) and activated in the furnace at 850°C for 2 h under a constant N₂ flow rate (10 mL min⁻¹) using a heating rate of 5°C min⁻¹ (AC_{ZnCl₂-850}). After activation, the obtained material was washed with HCl 0.1 M under stirring, and later with distilled water under vacuum filtration up to neutral pH. Finally, the washed sample was dried overnight at 105°C [12].

2.3 Activated carbon characterization

The point of zero charge (pH_{pZC}) was evaluated according to the method described by Carabineiro et al. [31]. Briefly, 20 mg of AC_{ZnCl₂-850} was put in contact with 20 mL of a 0.01 M NaCl solution at 200 rpm for 48 h to assure equilibrium. The pH of solutions was adjusted between 2 and 12 by adding HCl or NaOH with concentrations between 0.5 and 2 M.

The pore volume, surface area, and structural properties of AC_{ZnCl₂-850} were characterized by N₂ and CO₂ adsorption isotherms using an ASAP 2020 sorption analyzer

(Micromeritics). N₂ and CO₂ adsorption isotherms were recorded at -196°C and 0°C, respectively. Before measurements, a degassing procedure was carried out under vacuum at 300°C for 1 h. N₂ and CO₂ surface areas were determined using the Brunauer-Emmet-Teller (BET) equation and the mesopore volume and pore size distribution were determined by Barrett-Joyner-Halenda desorption isotherm. Total pore volume was determined at a relative pressure of 0.99 and this value was used to calculate micropore volume on the basis of mesopore volume neglecting the macropore volume (from the BJH equation) [19].

AC_{ZnCl₂-850} was analyzed by a scanning electron microscope coupled with EDX (ZEISS EVO LS 15 microscope) to study its morphological features and to determine its elemental composition before and after adsorption. Additionally, Fourier transform infrared (FTIR) spectra of AC_{ZnCl₂-850}, before and after adsorption were recorded with a VARIAN FTIR 670 spectrometer to characterize the fundamental sample functional groups.

2.4 Adsorption kinetic experiments

To optimize the adsorption process, batch experiments were performed at different pH (2, natural pH, 7, 9, and 12), initial dye concentration (5, 25, and 500 mg L⁻¹), and adsorbent dose (0.1–4.0 g L⁻¹) to study the removal of acid blue, red, and black industrial wood dyes by the AC_{ZnCl₂-850} prepared. An agitation speed of 210 rpm and a temperature of 25°C were ensured by a shaking water bath (H2O SOW-LAUDA). Samples were withdrawn at predefined times and centrifuged (Centronic, P Selecta) for 15 min at 4000 rpm. Dye concentration was determined by measuring the absorbance of the supernatant at the maximum dye wavelength, λ_{max}, using a UV/VIS spectrophotometer (V-630, Jasco), namely 602 nm and 572 nm for blue and black dyes, respectively, and for the red one at 506 nm from pH 2 to 7, 499 nm at pH 9 except at 500 mg L⁻¹ which maintains at 506 nm and 483 nm at pH 12.

The sorption efficiency was calculated using Eq. (1) as the percentage of dye adsorbed. The amount of dye adsorbed in mg g⁻¹ was calculated following Eq. (2).

$$\% \text{ Adsorption} = (C_0 - C)/C_0 \times 100 \quad (1)$$

$$q = (C_0 - C)V/m \quad (2)$$

where C₀ and C are the initial and residual dye concentrations (mg L⁻¹), q is the adsorption capacity (mg g⁻¹), V is the volume of the dye solution (L), and m is the dry mass of adsorbent used (g).

The kinetic models applied for the study of the adsorption process and the interaction mechanisms were the pseudo-first-order and pseudo-second-order kinetic models and the intraparticle diffusion model.

The pseudo-first-order kinetic model is related with the solid capacity and solution concentration and is applicable only during the initial stage of the adsorption process. It is given by:

$$\log(q_e - q_t) = \log q_e - k_1 t / 2.303 \quad (3)$$

where q_t and q_e are the amounts of dye adsorbed (mg g^{-1}) at time t (min) and at equilibrium, respectively, and k_1 represents the first-order rate constant (min^{-1}) [32].

The pseudo-second-order kinetic model can predict the behavior over the whole range of the adsorption process, and it is based on a solid phase sorption, usually related with chemisorption mechanism [32, 33]. The linearized form of the model is:

$$t/q_t = (1/k_2 q_e^2) + t/q_e \quad (4)$$

where k_2 ($\text{g mg}^{-1} \text{min}^{-1}$) is the pseudo-second-order rate constant.

The intraparticle diffusion model distinguishes different diffusion mechanisms and usually four steps are described to control the rate of adsorption process. These include (1) molecular diffusion from the solution to a film layer encircling the adsorbent; (2) diffusion occurring from the film to particle surface; (3) migration inside the adsorbent particle by “surface diffusion” or “pore diffusion”; and (4) adsorption uptake by many interaction mechanisms such as chemisorption, physisorption, complexation, or ion exchange. The intraparticle diffusion equation is as follows:

$$q_t = k_{id} t^{1/2} + C \quad (5)$$

where C (mg g^{-1}) is the intercept and k_{id} is the rate constant of intraparticle diffusion ($\text{mg g}^{-1} \text{min}^{-1/2}$) [4, 34].

2.5 Adsorption equilibrium experiments

Equilibrium data were obtained through batch experiments in which 2 g L^{-1} of $\text{AC}_{\text{ZnCl}_2-850}$ for black and 4 g L^{-1} of $\text{AC}_{\text{ZnCl}_2-850}$ for blue and red dyes were added to $25\text{--}500 \text{ mg L}^{-1}$ of dye solution at $\text{pH} = 2$ and 25°C for the equilibrium time (48 h) for blue and red dyes and 12 h for black dye to assure stability.

Langmuir and Freundlich isotherm models were employed to analyze the experimental data since they are the most commonly used for the study of equilibrium data [35]. According to the Langmuir's isotherm model, the uptake of adsorbate molecules takes place on a homogeneous surface with a limited number of adsorption sites giving rise to the formation of a monolayer and not including the interaction between adsorbed molecules. The linearized isotherm equation is represented by Eq. (6).

$$C_e/q_e = C_e/q_m + 1/q_m K_L \quad (6)$$

where C_e (mg L^{-1}) is the equilibrium dye concentration, q_e (mg g^{-1}) is the amount of dye at equilibrium, q_m (mg g^{-1}), and K_L (L mg^{-1}) are the Langmuir constants related to adsorption capacity and adsorption energy, respectively.

Dimensionless constant separation factor or equilibrium parameter, one of the essential characteristics of this model, can be expressed by the following equation:

$$R_L = 1/(1 + K_L C_0) \quad (7)$$

where C_0 is the initial dye concentration (mg L^{-1}). R_L indicates if the adsorption process is irreversible, linear, or favorable accordingly with the R_L value, $R_L = 0$, $R_L = 1$, and $0 < R_L < 1$, respectively.

The Freundlich isotherm model assumes that multilayer adsorption occurs in a non-uniform way with different values of heat of adsorption and with variable affinity to heterogeneous surface. The linear form of Freundlich isotherm model is described as follows:

$$\ln q_e = \ln K_F + 1/n (\ln C_e) \quad (8)$$

where K_F (L mg^{-1}) indicates the adsorption capacity and $1/n$ the adsorption intensity. If $1 < n < 10$ indicates that adsorption is favorable, if $n < 1$ is irreversible and $n > 10$ is unfavorable [4, 5].

2.6 Statistical analysis

All the experiments were done in triplicate and the values averaged. The existence of significant differences among the results for adsorption efficiency of $\text{AC}_{\text{ZnCl}_2-850}$ for all dyes was analyzed. In this regard, the one-way analysis of variance (ANOVA) was used, followed by Tukey or T3 Dunnett test according to the significant level. All statistical tests were performed at a 5% significance level using IBM SPSS Statistics 25 software.

3 Results and discussion

3.1 Effect of concentration on the natural pH of dye solutions

Natural pH was determined for each dye at concentrations of 5, 25, and 500 mg L^{-1} and changes were noticed with increasing concentration, but more remarkably for the red dye (Table 1).

pH is an important parameter that could influence the adsorption process and the pH effect on the adsorption will be evaluated

Table 1 Natural pH for blue, black, and red dyes at different concentrations

Natural pH			
	5 mg L ⁻¹	25 mg L ⁻¹	500 mg L ⁻¹
Blue	6.0	5.1	6.6
Black	4.8	5.7	6.7
Red	5.1	6.7	9.0

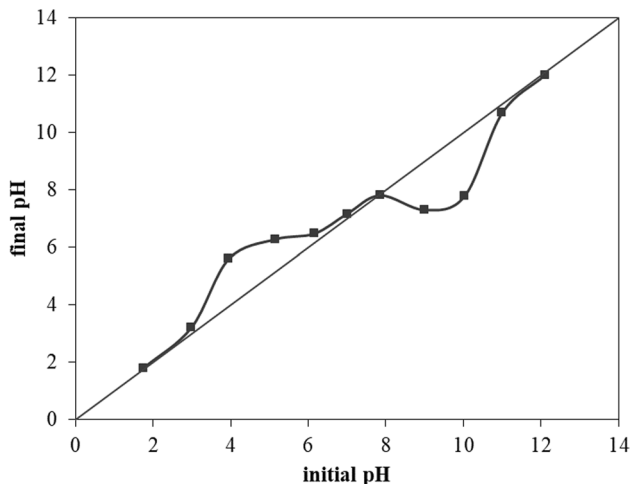


Fig. 1 Determination of pH_{PZC} for AC_{ZnCl2-850}

3.2 Activated carbon characterization before adsorption

The yield of AC_{ZnCl2-850} was calculated after activation and washing and it was 19.3±1.3% (based on pine sawdust on dry basis).

pH_{PZC} is the pH value at which the final pH is equal to the initial pH and represents when the net surface charge of the adsorbent is zero. Particularly, the pH_{PZC} reflects the acid or basic character of the adsorbent surface since the surface charge below the pH_{PZC} is positive and above this value is negative. Thus, pH_{PZC} is an important parameter to understand the interfacial properties and interactions during adsorption studies, indicating the ability of the activated carbon for the removal of anionic, cationic, or molecular pollutants since pH_{PZC} indicates the presence of acidic or basic surface functional groups [14, 15, 36]. Figure 1 shows the pH_{PZC} of the AC_{ZnCl2-850} to be 7.8.

This value falls in the basic region and the value of pH_{PZC} > 7 demonstrates the prevalence of basic groups over acidic groups. Acid wood dyes are negatively charged which implies that when the pH is lower than pH_{PZC}, the AC_{ZnCl2-850} could have more affinity with dyes.

BET surface areas were calculated from N₂ and CO₂ adsorption isotherms presented in Fig. 2, and with total and mesopore (2–50 nm) volumes and average pore diameter calculated from N₂ adsorption-desorption isotherm of the AC_{ZnCl2-850} are shown in Table 2.

Nitrogen adsorption-desorption isotherms of AC_{ZnCl2-850} show a reversible type I isotherm according to the IUPAC classification, suggesting that the carbon is particularly microporous since the significant uptake of N₂ at lower

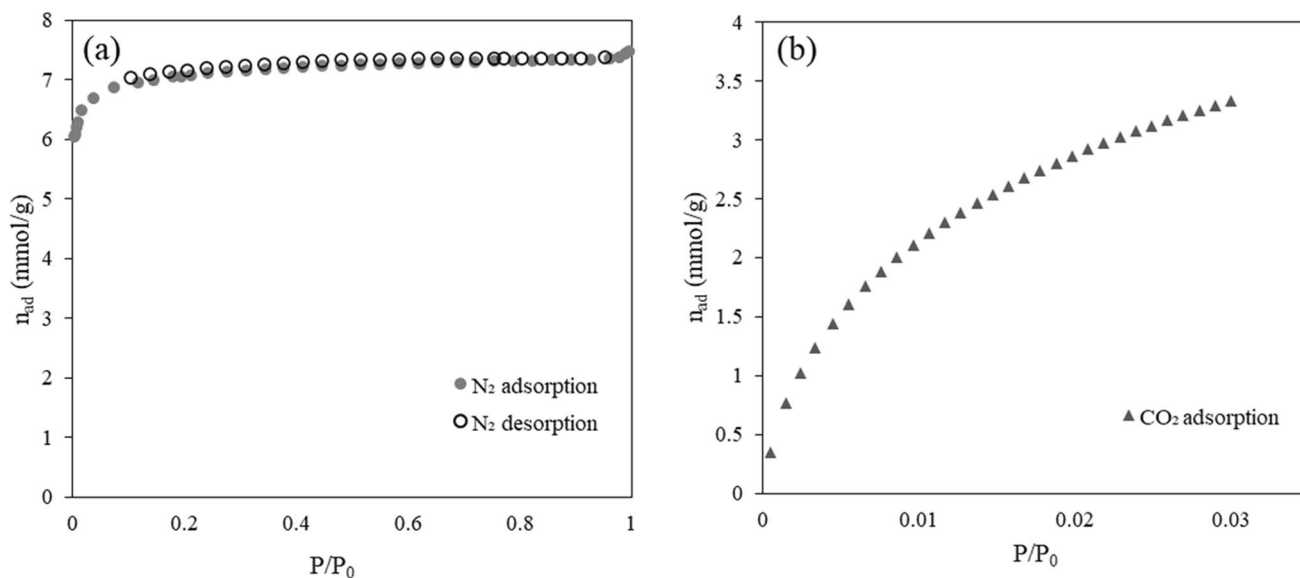


Fig. 2 Adsorption isotherms of (a) nitrogen and (b) carbon dioxide by AC_{ZnCl2-850}

Table 2 Surface characterization of the activated carbon prepared

Parameters	AC _{ZnCl₂-850}
BET surface area N ₂ (m ² g ⁻¹)	471.4
BET surface area CO ₂ (m ² g ⁻¹)	319.5
Total pore volume (cm ³ g ⁻¹)	0.26
Mesopore volume (cm ³ g ⁻¹)	0.03
Micropore volume (cm ³ g ⁻¹)	0.23
Average pore diameter (nm)	2.26

pressures is characteristic for the adsorption in micropores [37]. The initial sharp uptake could be also related with the presence of small mesopores [16]. Type I isotherms can be further subdivided into two types, I(a) and I(b), and from the analysis of Fig. 2a, it can be concluded that, in this case, it corresponds to a type I(a) isotherm which is characteristic of materials with pore size smaller than 1 nm [37, 38]. Additionally, the low amount of nitrogen adsorbed on the surface in the range of partial pressures used for BET area determination is related to the existence of a low surface area (Table 2). Previous studies have shown similar or higher surface area values in activated carbons produced from wood-based biomass [10]. Furthermore, the surface analysis has been completed by performing CO₂ adsorption (Fig. 2b) since the N₂ adsorption-desorption isotherms analysis can be limited due to micropore presence and low diffusivity [39]. The high CO₂ adsorption capacity, in comparison with similar fabricated carbons [9, 40], can be attributed to the activated carbon microporous nature. In addition, the low value of the surface area determined by nitrogen adsorption in comparison with the corresponding CO₂ surface area indicates an important presence of ultramicroporosity (pore diameter lower than 0.7 nm), together with a significant presence of micropores (with pore diameters higher than 0.7 nm) and low amount of mesopores. This pore size distribution agrees with the average pore size of the carbon [41–43].

The high microporosity percentage (91%) combined with the high BET surface area calculated with CO₂ reveals the important role of microporosity on gas adsorption. This percentage also indicates that the chemical activation process generates a high-quality carbonaceous material in which micropores are predominant [25].

The type of starting material and carbonization and activation conditions are the most important factors that influence the features of activated carbon porosity [7]. The total surface area of AC_{ZnCl₂-850} is 471.4 m² g⁻¹ of which 91% corresponds to micropores (< 2 nm) due to the effect of ZnCl₂ on micropore formation that inhibits the development of tar and favors the release of volatiles [35, 36]. Moreover, as seen the activated carbon prepared

with ZnCl₂ as chemical activator has a well-developed microporosity. A preceding study on the preparation of activated carbon from *Eucalyptus camaldulensis* wood showed that the type of activation agent and its concentration influence the surface area and pore volume and the BET surface area and porosity increased in the subsequent order: KOH > H₃PO₄ > ZnCl₂. ZnCl₂ and its hydrates mainly cause the formation of small and uniform size micropores due to its minuscule particle size [10, 16]. Previous studies using agricultural wastes with the same activation agent reported similar values for surface area [5, 19] and microporosity [14, 44].

SEM micrographs of AC_{ZnCl₂-850} are presented in Fig. 3. The development of pores was observed in the activated carbon prepared, suggesting a high surface area and supporting the information provided by the surface area and porosity analysis. As mentioned before, the pores on the surface of the carbon were probably due to the ZnCl₂ evaporation during the activation process and to the catalytic effect of the ZnCl₂ on the pyrolytic decomposition [15]. Moreover, the SEM image at 1000× magnification (Fig. 3a) shows a prominent honeycomb structure originated from the cell wall of the raw sawdust [5, 12].

The elemental composition of AC_{ZnCl₂-850} is shown in Table 3. High carbon content is observed that may be due to the decomposition of cellulose and hemicelluloses (between 200 and 400°C) and lignin (between 150 and 750°C) [10, 15]. Oxygen, one of the main components of sawdust, showed the opposite behavior. The presence of zinc and chloride atoms indicates that during the activation process, ZnCl₂ reacted with PS revealing the activation efficiency [14, 45].

Up to now, various papers can be found in literature on ZnCl₂-activated carbons from biomass feedstocks, but apparently none of them prepared through a dry activation process by milling, but through impregnation with a ZnCl₂ dissolution [7, 11]. Therefore, it can be concluded that the dry activation technique is also efficient, faster, and with no formation of aqueous chemical residues. EDX results after adsorption will be discussed in Section 3.3.5.

To obtain a greater insight into the functional groups on the surface of the material before and after adsorption, the FTIR spectra were collected. The FTIR spectra of AC_{ZnCl₂-850} before and after dye adsorption are shown in Fig. 4.

The occurrence of a strong and broad peak around 3400 cm⁻¹ which is ascribed to a stretching vibration of hydrogen-bonded (O-H) hydroxyl groups from carboxyl, phenols, alcohols, or surface bonded water is observed. The adsorption small bands between 2919 and 2852 cm⁻¹ correspond to asymmetric and symmetric C-H stretching vibrations of alkyl side chains. The two small peaks around 2300 cm⁻¹ could be attributed to the alkyne group

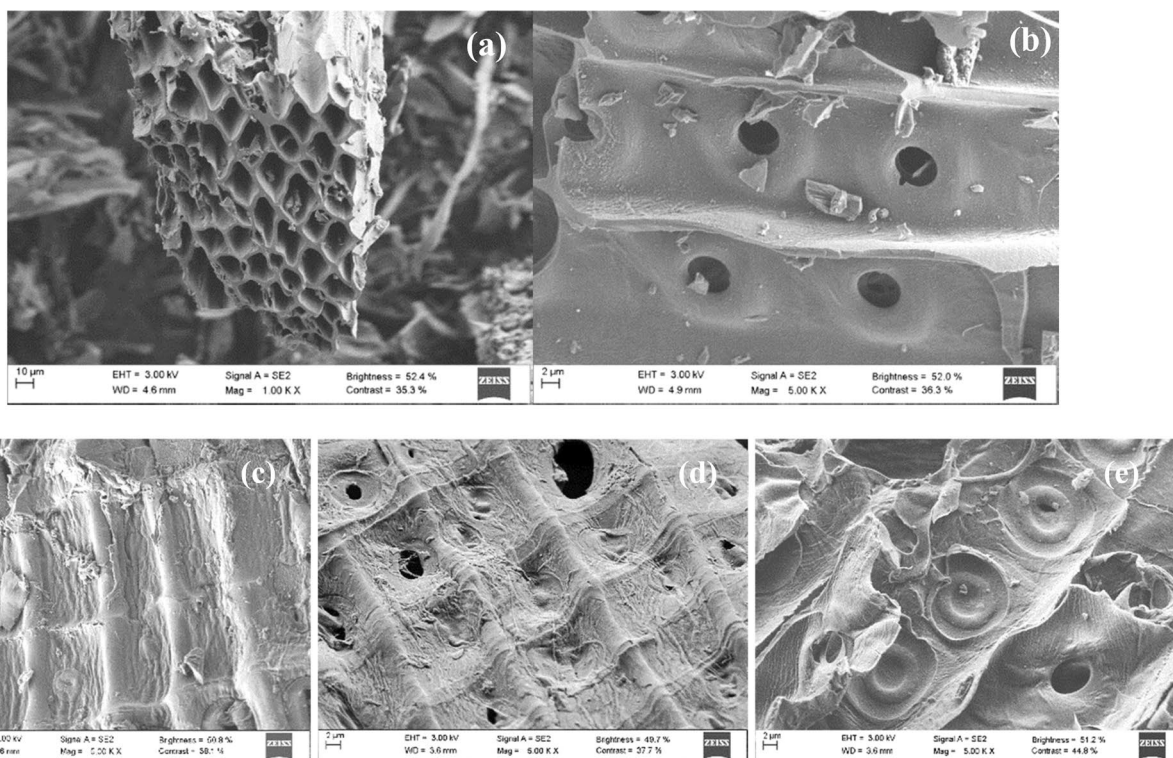


Fig. 3 SEM images of AC_{ZnCl2-850} at (a) 1000 and (b) 5000× magnifications before adsorption and after adsorption with (c) blue, (d) red, and (e) black wood dyes (500 mg L⁻¹; pH = 2; adsorbent dose: 0.4

g L⁻¹ for blue, 0.5 g L⁻¹ for red, and 1 g L⁻¹ for black dyes; contact time: 48 h for blue and red dyes and 12 h for black dye; temperature: 25 °C; agitation speed: 210 rpm) at 5000×

Table 3 Elemental composition of dyes and AC_{ZnCl2-850} before and after adsorption (500 mg L⁻¹; pH = 2; adsorbent dose: 0.4 g L⁻¹ for blue, 0.5 g L⁻¹ for red, and 1 g L⁻¹ for black; contact time: 48 h for blue and red dyes and 12 h for black dye; temperature: 25 °C; agitation speed: 210 rpm)

wt%	AC _{ZnCl2-850}	Blue dye	Black dye	Red dye	AC _{ZnCl2-850} +blue dye	AC _{ZnCl2-850} +black dye	AC _{ZnCl2-850} +red dye
C	90.4	62.1	27.5	49.7	90.7	92.7	93.3
O	2.6	18.4	18.4	28.3	7.2	5.2	4.1
Zn	2.3	-	-	-	0.6	-	-
S	2.1	6.7	21.3	7.1	1.8	0.1	0.2
F	1.6	-	-	-	-	-	-
Cl	0.6	0.4	-	0.9	0.9	1.8	2.3
Si	0.1	-	-	-	0.1	0.03	0.03
Ca	0.1	-	-	-	0.3	0.1	0.1
N	-	7.2	-	3.4	-	-	-
Na	-	4.8	11.1	10.1	-	-	-
Br	-	0.2	-	-	-	-	-
Cu	-	0.1	1.6	0.1	0.1	0.2	0.3
P	-	-	-	0.4	-	-	-
Cr	-	-	20.0	-	-	0.1	-
Mg	-	-	0.1	-	-	-	-

(C≡C). The spectral bands at 1650 and 1540 cm⁻¹ correspond to the C=C aromatic ring. Likewise, the small band at 1380 cm⁻¹ is associated to C=C stretching aromatic rings polarized by oxygen atoms bound near of the carbon atoms [16, 37]. Finally, a broad band at 1047 cm⁻¹ is assigned to C-O stretching alcohols.

3.3 Adsorption experiments

3.3.1 Effect of pH

Initial pH plays an essential role in the adsorption process, affecting not only the chemistry of dye molecules but also

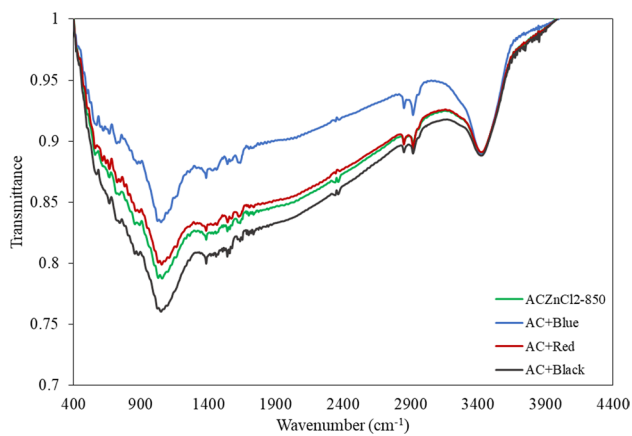


Fig. 4 FTIR spectra of AC_{ZnCl_2-850} before and after adsorption with blue, red, and black dyes (500 mg L^{-1} ; $\text{pH} = 2$; adsorbent dose: 0.4 g L^{-1} for blue, 0.5 g L^{-1} for red, and 1 g L^{-1} for black dyes; contact time: 48 h for blue and red dyes and 12 h for black dye; temperature: 25°C ; agitation speed: 210 rpm)

the carbon surface binding sites [4, 33]. The pH effect was evaluated (Fig. 5) at an initial dye concentration of 5 mg L^{-1} , an adsorbent dose of 0.5 g L^{-1} , and a contact time of 48 h to assure equilibrium, except for the black dye that was not stable for times greater than 12 h as determined in a previous work (accepted for publication).

Figure 5 shows that the total removal of the blue dye was achieved at all pH values essayed. For the red dye, the highest removal was obtained at $\text{pH} = 2$ (96.8%) and natural pH (96.0%) but decreased when pH was increased from 7 to 12. Regarding the black dye, the removal percentages were much lower than those for the red and blue ones. The greatest elimination was achieved at $\text{pH} = 2$ (55.6%) and progressively fell by increasing pH from 2 to 12. Possibly,

the increase of dye adsorption at pH lower than pH_{PZC} is because the activated carbon surface is positively charged and becomes highly protonated; hence, acid dye anion adsorption increases through electrostatic attraction and hydrogen bonding [4, 5]. Therefore, according to these results, the influence of the adsorbent dose was analyzed at the most favorable pH, natural pH for blue and red dyes, and $\text{pH} = 2$ for the black one.

In a previous study (accepted for publication), the removal of wood dyes by pine (*Pinus radiata*) sawdust was evaluated as function of pH. It was found that at an initial dye concentration of 5 mg L^{-1} and the optimum conditions ($\text{pH} = 2$ and an adsorbent dose of 6 g L^{-1}), adsorption capacities of 0.70, 0.75, and 0.72 mg g^{-1} and removal percentages of 100, 92.4, and 99% were obtained for the blue, red, and black dyes, respectively. It is important to point out that the values of adsorption performance depend on the conditions used and it is not possible to compare them directly. In addition, the removal of the three dyes by pine sawdust biochar at the same conditions than for AC_{ZnCl_2-850} (5 mg L^{-1} , $\text{pH} = 2$, adsorbent dose of 0.5 g L^{-1}) was analyzed and maximum adsorption capacities of 2.13, 2.55, and 1.94 mg g^{-1} and removal percentages of 19.7, 25.1, and 23.2% for blue, red, and black dyes, respectively, were achieved. These results confirm the efficacy of the activation process, since the adsorption capacities for PS and biochar were lower than for AC_{ZnCl_2-850} (10.15 , 9.36 , and 5.52 mg g^{-1} for blue, red, and black, respectively).

3.3.2 Effect of adsorbent dose

The effect of adsorbent dose on dye adsorption was studied and the results are presented in Fig. 6. For the blue and red dyes that showed high removal efficiencies at natural pH

Fig. 5 Effect of pH on adsorption of blue, red, and black wood dyes onto AC_{ZnCl_2-850} (natural pH: 6.0, 5.1, and 4.8 for blue, red, and black dyes, respectively; dye initial concentration: 5 mg L^{-1} ; adsorbent dose: 0.5 g L^{-1} ; contact time: 48 h for blue and red dyes and 6 h for black dye; temperature: 25°C ; agitation speed: 210 rpm). For each dye, different letters indicate significant differences ($p \leq 0.05$) between samples

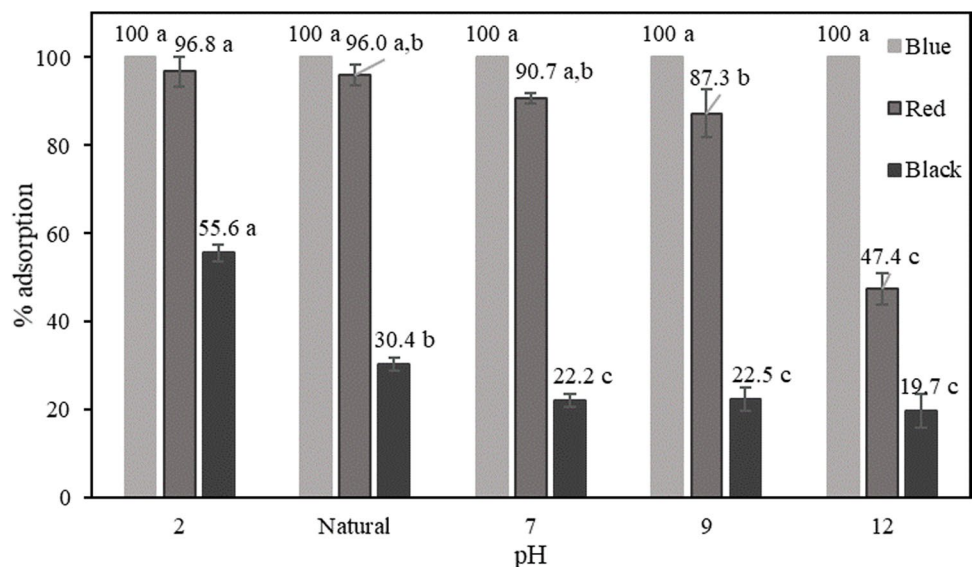
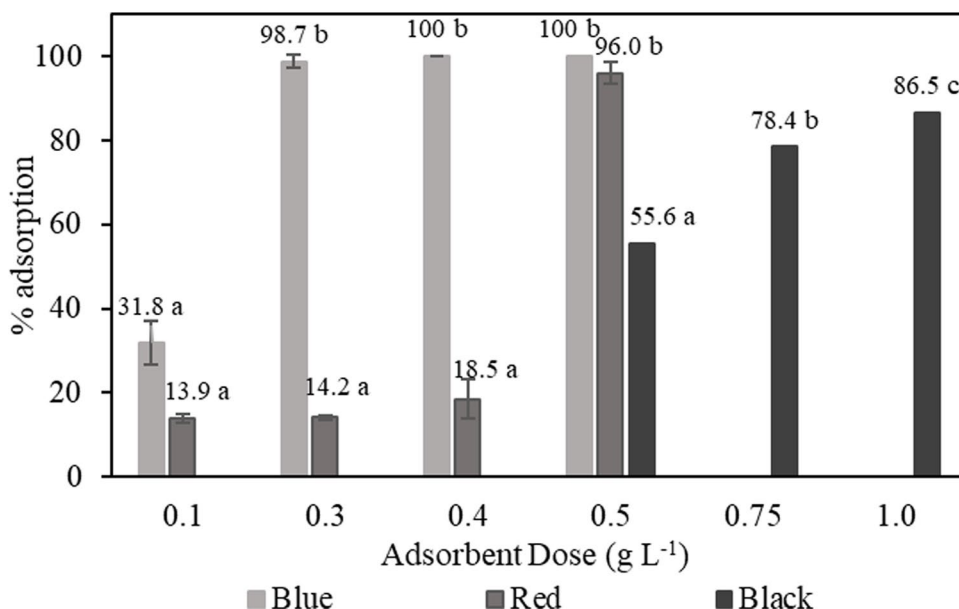


Fig. 6 Effect of adsorbent dose on adsorption of blue, red, and black wood dyes onto AC_{ZnCl_2-850} (pH: 6.0 and 5.1 for blue and red dyes respectively and pH = 2 for black dye; dye initial concentration: 5 mg L^{-1} ; contact time: 48 h for blue and red dyes and 6 h for black dye; temperature: 25°C ; agitation speed: 210 rpm). For each dye, different letters indicate significant differences ($p \leq 0.05$) between samples



and 5 mg L^{-1} , the adsorbent dose was reduced to 0.1 g L^{-1} . For the black dye, given the poor results at 0.5 g L^{-1} , the adsorbent dose was increased up to 1.0 g L^{-1} .

For the blue colorant, a 100% removal percentage was maintained by reducing the dose from 0.5 to 0.4 g L^{-1} , but there was a significant decrease to 31.8% when the adsorbent dose was lowered to 0.1 g L^{-1} . Regarding the red colorant, it was not possible to reduce the adsorbent dose ensuring the total removal of dye since the percentage decreased to 18.5% and 14.0% at 0.4 g L^{-1} and 0.1 g L^{-1} , respectively. Finally, for the black dye, an increase in the adsorbent dose from 0.5 to 0.75 and 1.0 g L^{-1} increased the dye removal percentage from 55.6 to 78.4% and 86.5%, respectively. In general, this behavior can be explained by the increase of the adsorption sites available with increasing the adsorbent dose, and by a high ratio of dye molecules to empty sites [4, 33]. Regarding the equilibrium adsorption capacity (q_{max}), it decreased from 17.2 to 10.2 mg g^{-1} for the blue and from 9.3 to 6.8 mg g^{-1} for the red with increasing the adsorbent dose from 0.1 to 0.5 g L^{-1} . For the black dye, q_{max} decreased from 5.5 to 4.2 mg g^{-1} with increasing the adsorbent dose from 0.5 to 1 g L^{-1} .

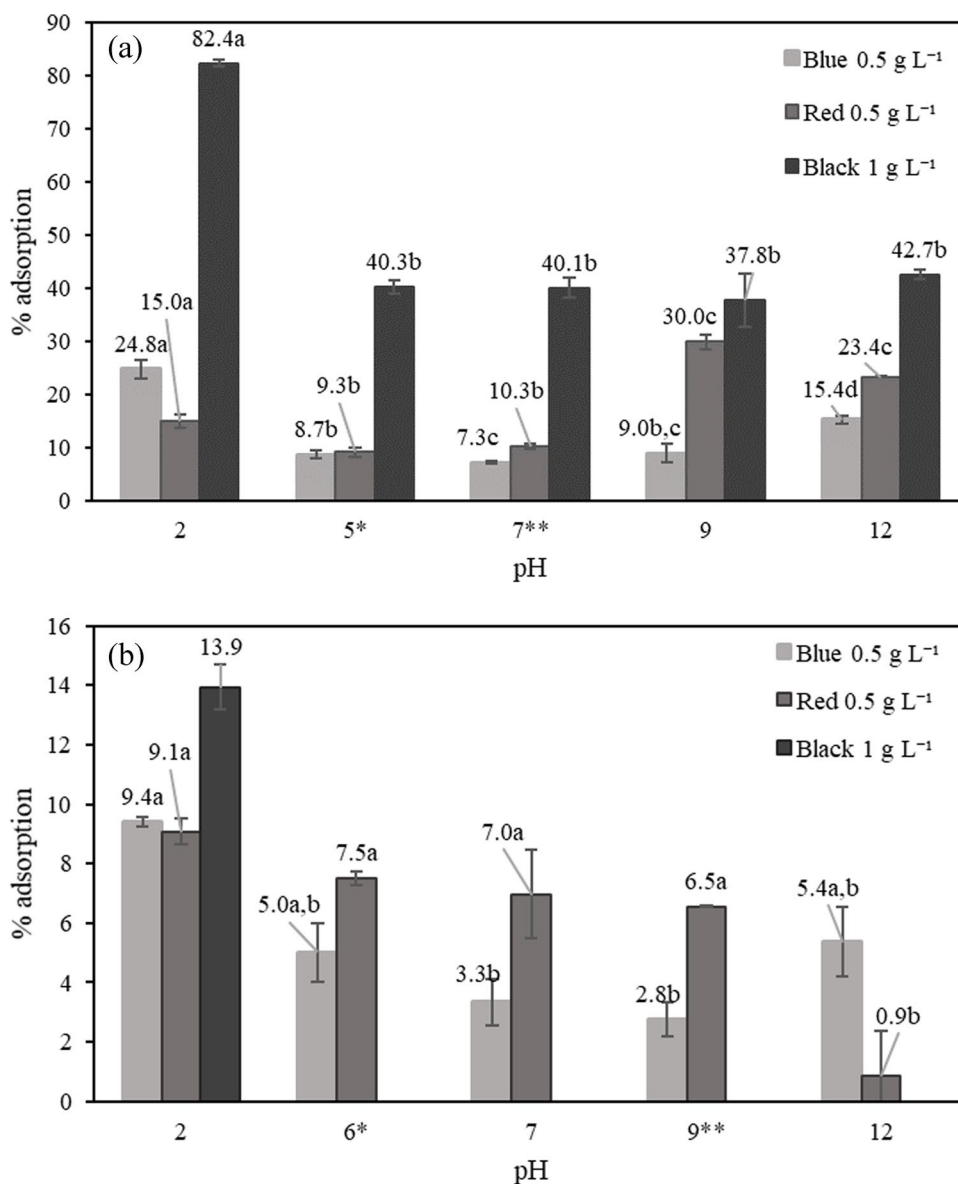
3.3.3 Effect of initial dye concentration

The influence of the initial dye concentration (25 and 500 mg L^{-1}) on dye removal at different pH was studied at the adsorbent doses selected from the previous experiments (0.5 g L^{-1} for the blue and the red dyes and 1 g L^{-1} for the black one) and the obtained results are presented in Fig. 7. Adsorption percentage decreased with increasing initial dye concentration due to the saturation of the adsorbent surface while adsorption capacity increased due to the higher concentration gradient which acts as a driving force to overcome

resistances to dye mass transfer between the aqueous phase and the solid phase [46].

With respect to the blue wood dye, the highest adsorption percentages were obtained at pH = 2 at both initial dye concentrations and the maximum adsorption capacity was 6.27 and 97.56 mg g^{-1} for 25 and 500 mg L^{-1} , respectively. Regarding the red dye, the natural pH increased significantly with increasing the initial dye concentration (Table 1). Therefore, the higher removal percentage occurred at different pH depending on initial dye concentration and decreased with increasing dye concentration. It was 30% at pH = 9 for 25 mg L^{-1} with an adsorption capacity of 16.46 mg g^{-1} and 9.1% at pH = 2 for 500 mg L^{-1} with an adsorption capacity of 86.61 mg g^{-1} . As mentioned above, usually when the pH is less than pH_{PZC} , there will be more H^+ ions and will balance the charge of anionic groups in the adsorbent surface favoring anionic adsorption due to an electrostatic interaction and hydrogen bonding. At 25 mg L^{-1} , this behavior was not verified which suggests that the adsorption process is probably ascribed to other mechanisms [20]. In previous work above mentioned, it was found that the pKa for these dyes is around 10 which means that pH = 9 is above the pH_{PZC} and below the pKa, then, the molecules are protonated and Lewis acid-base, π - π bond, or hydrophobic effects could also occur [47]. For the black dye, at 25 mg L^{-1} , the maximum removal (82.4%) was obtained at pH = 2 with an adsorption capacity of 19.71 mg g^{-1} , following the same trend with the pH increase as for the low concentration. Then, the initial concentration was increased to 500 mg L^{-1} at pH = 2 and the removal percentage decreased to 13.9% with an adsorption capacity of 62.73 mg g^{-1} . Similar results in which the removal percentage decreased with

Fig. 7 Effect of initial dye concentration at different pH values on adsorption of blue, red, and black wood dyes onto AC_{ZnCl_2-850} at (a) 25 mg L^{-1} and (b) 500 mg L^{-1} (natural pH at 25 mg L^{-1} : *5.1, **6.7, and *5.7; natural pH at 500 mg L^{-1} : *6.6 and **9.0 for blue and red dyes, respectively; contact time: 48 h for blue and red dyes and 12 h for black dye; temperature: 25°C ; agitation speed: 210 rpm). For each dye, different letters indicate significant differences ($p \leq 0.05$) between samples



increasing the initial dye concentration have been reported in literature for dyes removal by activated carbons [4, 44].

In view of the good results obtained for the blue and red dyes with 5 mg L^{-1} and $\text{pH} = 2$ at an adsorbent dose at 0.5 g L^{-1} (Fig. 5), the initial concentration was increased maintaining the dose and a considerable decrease in the adsorption efficiency was obtained as seen in Fig. 7. Then, the effect of the adsorbent dose ($0.5, 1, 2,$ and 4 g L^{-1}) was analyzed for an intermediate concentration of 25 mg L^{-1} . For both dyes, the removal percentage increased to around 55% using 1 g L^{-1} , and to 91 and 95% for blue and red dyes, respectively, with 2 g L^{-1} , and the complete removal was achieved for 4 g L^{-1} , as observed in Fig. 8.

For the black dye, in an attempt to achieve the total dye removal for an intermediate concentration of 25 mg L^{-1}

and $\text{pH} = 2$, the adsorbent dose was increased to 2 g L^{-1} . This increase in the adsorbent dose was effective since it increased the dye removal percentage from 82.4 to 98.1% with complete color removal (Fig. 8). As mentioned before, the increase on the adsorption percentage can be related with the surface area and the availability of more adsorption sites.

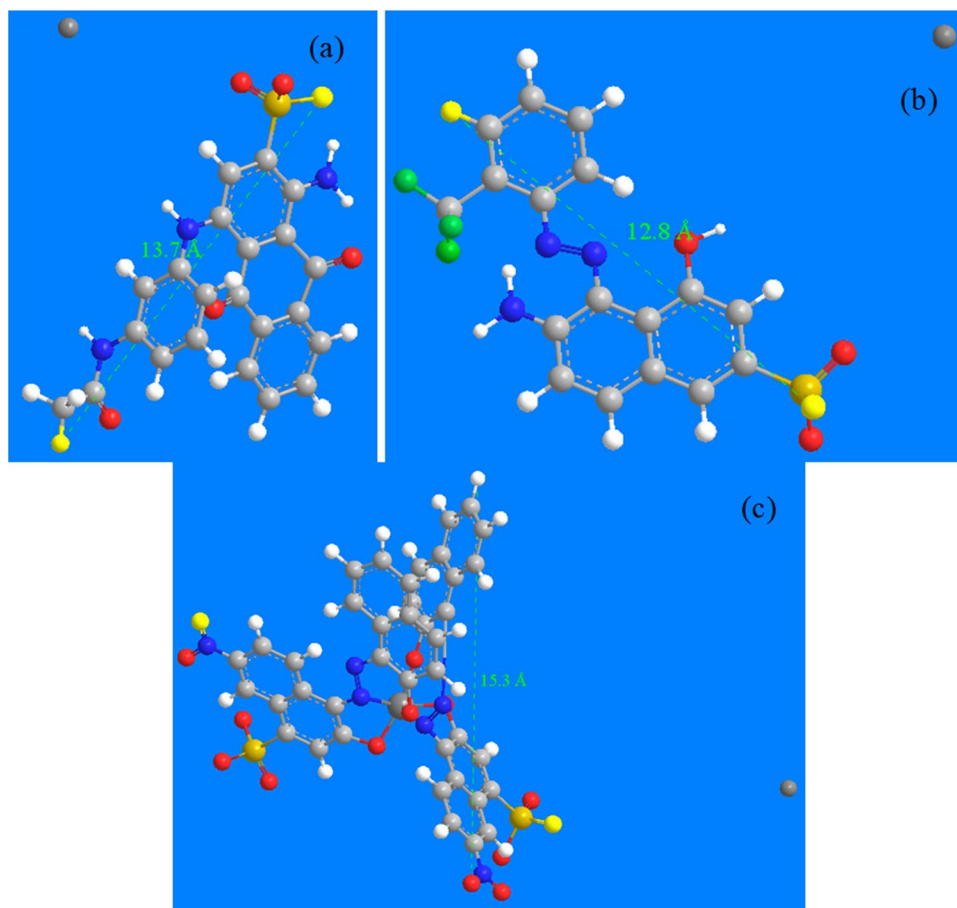
Additionally, in order to check the existence of size exclusion affecting dye adsorption, the highest distance between two extreme atoms of each dye molecule was measured through ChemDraw 21.0.0 software. These values, shown in Fig. 9, were 1.37, 1.28, and 1.53 nm for blue, red, and black dyes, respectively, which are lower than carbon average pore diameter, 2.26 nm (Table 2), although the important presence of microporosity (91%) should be considered. In addition, the value of surface area determined with CO_2 at 0°C ($319.5 \text{ m}^2 \text{ g}^{-1}$) indicates



Fig. 8 Effect on color intensity with the maximum dose of adsorbent on dye removal (pH = 2; initial dye concentration: 25 mg L⁻¹; adsorbent dose: 4 g L⁻¹ for blue and red dyes and 2 g L⁻¹ for black; contact

time: 48 h for blue and red dyes and 12 h for black dye; temperature: 25°C; agitation speed: 210 rpm)

Fig. 9 Chemical structures with distance between two extreme atom measurements of (a) blue dye, (b) red dye, and (c) black dye (H = white, C = grey, N = blue, S = yellow, O = red, F = green, Na = dark grey)



the high presence of pores in the ultramicroporosity range (lower than 0.7 nm) which hinders the access of the dye molecules. Therefore, considering the results found in this work, where for given conditions the adsorption

performance depended on the dye essayed, it cannot be concluded that only limitation by sizes exists but distinct interactions between the carbon and the different dye molecules.

3.3.4 Adsorption kinetics

The pseudo-first-order, pseudo-second-order, and intraparticle diffusion models were employed at the conditions selected to elucidate the mechanisms of the adsorption process. The fitting results of the experimental data of adsorption of blue, black, and red dyes onto AC_{ZnCl_2-850} adsorbent using pseudo-first-order, pseudo-second-order, and intraparticle diffusion models are shown in Fig. 10. The obtained results for kinetic parameters and correlation coefficient (R^2) are shown in Table 4.

The R^2 values for the pseudo-second-order kinetics model were higher than 0.999 and the calculated adsorption capacities ($q_{e,calc}$) were close to the experimental ones ($q_{e,exp}$) which revealed that kinetic data were best fitted to this model, an indication of a chemisorption mechanism.

Regarding the intraparticle diffusion model, in which the adsorption of soluble species from a solution involves their transfer to the surface of an adsorbent, as evident from Fig. 10c, the linear plots presented multilinearity, indicating that the adsorption occurs in two steps and that the

intraparticle diffusion was not the only process that controlled the adsorption [33]. Usually, the first corresponds to the molecular diffusion of adsorbate through the bulk solution to the external surface of the adsorbent originating a film layer. The second one implies the migration by intraparticle diffusion into the adsorbent pores until the final equilibrium stage [4, 6, 26, 44]. Based on the R^2 values (> 0.9) presented in Table 4, for the first stage dye adsorption, the experimental data are well fitted to the intraparticle diffusion model. Moreover, C value is proportional to the extent of the boundary layer thickness and in this case, as it is higher than 0 means that intraparticle diffusion is not the only rate-controlling step and implies a certain controlling degree of film diffusion and rapid adsorption [46].

The adsorption capacity of distinct adsorbents varies according to the primary source of the adsorbent, the process conditions of adsorption, adsorption modification, and the type of contaminant [48]. Nowadays is very important to find adsorbents with good adsorption capacity and low cost. Extensive research has been done and the adsorption capacity of activated carbons derived from wood for

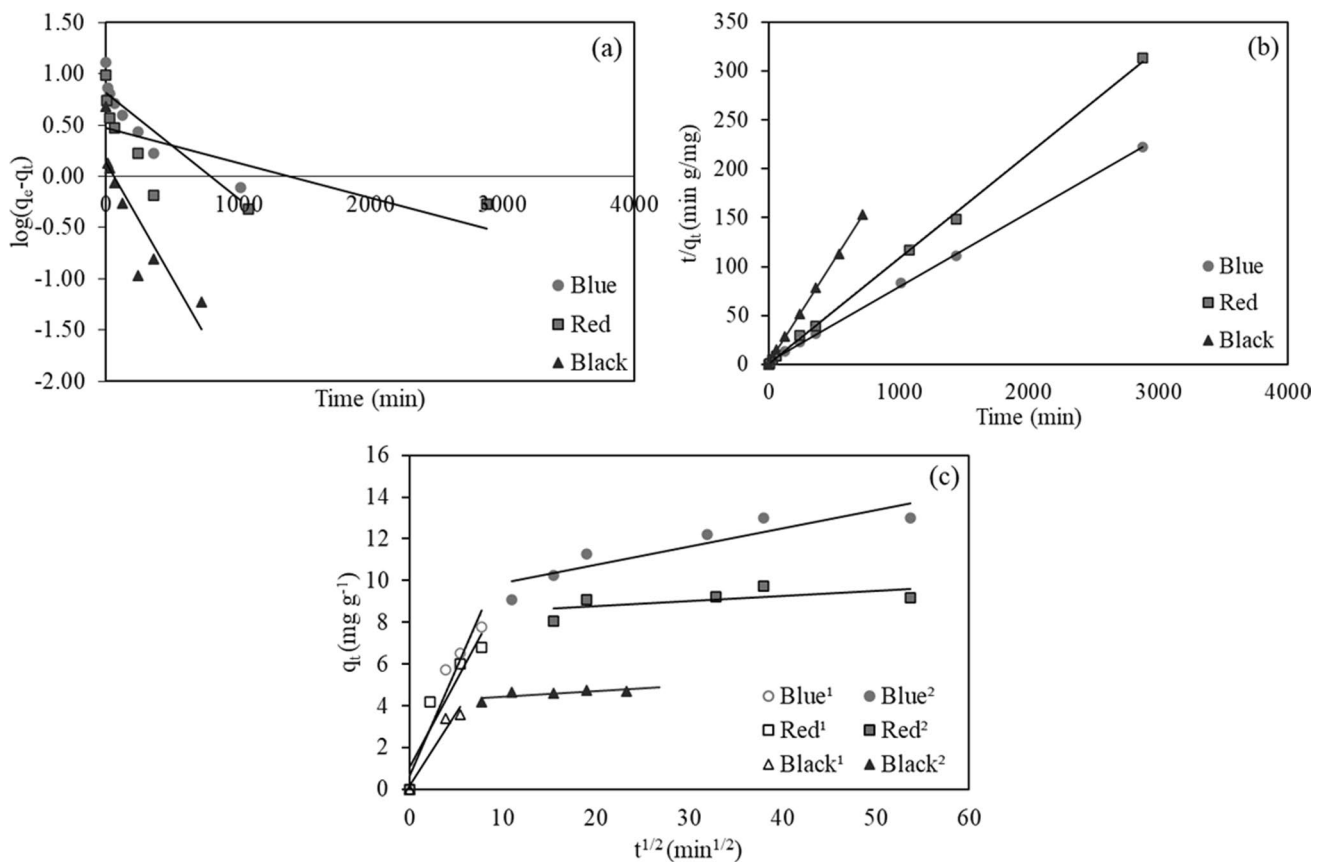


Fig. 10 (a) Pseudo-first-order, (b) pseudo-second-order, and (c) intraparticle diffusion (1: first stage and 2: second stage) kinetic plots (natural pH: 6.0 and 5.1 for blue and red dyes, respectively; pH = 2 for black dye; dye concentration: 5 mg L^{-1} ; adsorbent dose: 0.4 g L^{-1}

for blue, 0.5 g L^{-1} for red, and 1 g L^{-1} for black dyes; contact time: 48 h for blue and red dyes and 12 h for black dye; temperature: 25°C ; agitation speed: 210 rpm)

Table 4 Pseudo-first-order, pseudo-second-order, and intraparticle diffusion kinetic model parameters

Model	Parameter	Adsorption conditions		
		Blue 0.4 g L ⁻¹ natural pH	Red 0.5 g L ⁻¹ natural pH	Black 1.0 g L ⁻¹ pH = 2
Pseudo-first-order	$q_{e,exp}$ (mg g ⁻¹)	12.98	9.73	4.76
	$q_{e,calc}$ (mg g ⁻¹)	6.57	4.14	1.36
	k_1 (min ⁻¹)	2.30·10 ⁻³	2.30·10 ⁻³	5.30·10 ⁻³
	R^2	0.825	0.704	0.754
Pseudo-second-order	$q_{e,calc}$ (mg g ⁻¹)	13.12	9.33	4.77
	k_2 (g mg ⁻¹ min ⁻¹)	1.92·10 ⁻³	1.17·10 ⁻²	2.44·10 ⁻²
	R^2	0.999	0.999	1.000
Intraparticle diffusion	$k_{id,1}$ (mg g ⁻¹ min ^{-1/2})	1.02	0.83	0.69
	C_1 (mg g ⁻¹)	0.65	1.05	0.17
	R^2	0.934	0.876	0.937
	$k_{id,2}$ (mg g ⁻¹ min ^{-1/2})	8.78·10 ⁻²	2.43·10 ⁻²	2.70·10 ⁻²
	C_2 (mg g ⁻¹)	8.99	8.29	4.18
	R^2	0.812	0.381	0.584

Table 5 Comparison of the adsorption capacities of activated carbons prepared from various wood-based biomass for dye removal

Precursor	Adsorbate	Adsorption capacity (mg g ⁻¹)	Reference
Pine sawdust	Blue for wood	12.98	Present work
Pine sawdust	Red for wood	9.73	Present work
Pine sawdust	Black for wood	4.76	Present work
<i>Ailanthus altissima</i> wood	Acid blue 1	0.453	[49]
Outer rind of wood apple	Crystal violet	19.8	[50]
Outer rind of wood apple	Methylene blue	40.1	[50]
Poplar wood	Acid red 18	3.91	[51]
Wood apple outer shell	Methylene blue	35.1	[52]
<i>Acacia mangium</i> wood	Methyl orange	7.54	[53]
Oak wood	Malachite green	4.34	[54]
Peanut sticks wood	Methylene blue	2.57	[55]
Poplar wood	Acid red 18	3.91	[26]
<i>Citrus limon</i> wood	Crystal violet	23.6	[48]

dye adsorption is compared in Table 5 with those of the present work. Otherwise, Table 6 compares the kinetic modeling of dye adsorption onto ZnCl₂-activated carbons from biomass.

3.3.5 Activated carbon characterization after adsorption

SEM-EDX technique was employed after adsorption to compare the surface physical morphology and elemental

analysis of the materials with the original one. Figure 3 also shows the SEM photographs of the AC_{ZnCl₂-850} after adsorption with blue, red, and black dyes, respectively, at pH = 2 and the highest dye initial concentration essayed.

The SEM images showed that the surface of the carbon was changed due to the binding of dye molecules. It is observed that the pores were occupied by dyes that formed a slight cover over the entire surface, which was confirmed by comparing EDX analysis before and after adsorption. The EDX results shown in Table 3 reflect that after adsorption, in all cases, the amounts of C and O increased with respect to the original activated carbon. In addition, Cu and Cr atoms present in dye composition appear in AC_{ZnCl₂-850}, evidencing the adsorption of dye molecules to the activated carbon surface.

The FTIR spectrum of the activated carbon before and after dye adsorption is pretty similar but modifications in the intensity of several peaks appeared (for instance between 2919 and 2852 and at around 2300, 1650, 1540, and 1047 cm⁻¹), demonstrating that the activated carbon functional groups such as carboxyl, phenols, alcohols, or alkynes participated in the adsorption mechanism. Previous studies demonstrated that functional groups containing oxygen of carboxylic and carbonyl species enhance the adsorption of methylene blue dye molecules due to electrostatic interaction [8].

3.3.6 Adsorption equilibrium

To analyze the adsorption equilibrium, the Langmuir and Freundlich models were applied (Fig. 11) and the calculated parameters are listed in Table 7.

Table 6 Various kinetic and isotherm studies for dye adsorption onto ZnCl₂-activated carbon from biomass

Raw material	Dye	Kinetic model	Isotherm model	Reference
Pine sawdust	Blue for wood; Black for wood	Pseudo-second-order and intraparticle diffusion	Freundlich	Present work
Pine sawdust	Red for wood	Pseudo-second-order and intraparticle diffusion	Langmuir	Present work
<i>Paulownia tomentosa</i> wood	Acid red 4; methylene blue	Pseudo-second-order	Langmuir	[24]
Mixture of orange peel and watermelon rind	Crystal violet; methylene blue	Pseudo-second-order	Freundlich	[16]
Mixture of carrot juice pulp and pomegranate peel	Crystal violet	Pseudo-second-order	Freundlich	[17]
Coconut shell	Malachite green	Intraparticle diffusion	Freundlich	[5]
Tomato processing	Methylene blue; metanil yellow	-	Langmuir	[35]
Pine sawdust	Malachite green	Pseudo-second-order and intraparticle diffusion	Langmuir	[44]
<i>Enteromorpha prolifera</i>	Reactive red 23; reactive blue 171; reactive blue 4	Pseudo-second-order	Freundlich	[57]
Cashew nut shells	Methylene blue	-	Langmuir	[37]
Shaddock peel	Methylene blue	Pseudo-second-order	Langmuir	[59]
Glycerine pitch distillate	Methylene blue	Pseudo-second-order	Langmuir and Redlich-Peterson	[46]

For the blue and black dyes, the Freundlich isotherm offered the better adjustment with values of the coefficient of determination (R^2) of 0.981 and 0.839, respectively (Table 7). The Freundlich model suggests the heterogeneity of the carbon surface with multilayer adsorption of dyes. Moreover, the values of n between 1 and 10 suggest a favorable adsorption. The removal of malachite green using ZnCl₂-activated carbon from coconut shell was also well described by the Freundlich model [5]. Regarding the Langmuir model, R_L values lower than 1 also indicated that dye adsorption was favorable.

Regarding the red dye, the equilibrium adsorption capacity was 12.89 mg g⁻¹ at 100 mg L⁻¹ and decreased with increasing dye initial concentration. Thus, the experimental equilibrium data in the range essayed were not suitable for isotherm modeling. This behavior can be related to observed pH changes with dye concentration, as pH affects the carbon's surface and, therefore, the adsorption capacity [56]. Even though, for dye concentrations below 100 mg L⁻¹, the isotherm models were tested (Fig. 11) and the calculated parameters are presented in Table 7. From these results, it can be clearly concluded that Langmuir model offers the best adjustment to the experimental data. Thus, red dye adsorption equilibrium differs from the other dyes, and, probably, monolayer adsorption occurs which can explain the maximum capacity reached at 100 mg L⁻¹ due to nearly complete coverage of the active sites [57]. Besides, the value of the dimensionless separation factor (R_L) between 0 and 1 indicates that the red dye adsorption onto this carbon is favorable. The Langmuir isotherm also explained the adsorption

equilibrium of Congo red dye onto *Bombax Buonopozense* bark-activated carbon [58]. Table 6 compares equilibrium modeling of dye adsorption onto ZnCl₂-activated carbon from biomass.

3.3.7 Adsorption mechanism of wood dyes onto activated carbon

The adsorption mechanism not only depends on the contaminant's properties but also on the surface chemistry of the adsorbent [3]. The key interactions found in literature for dye removal include electrostatic interaction, pore-filling, π - π interaction, and hydrogen bonding [16]. Some of these interactions may be involved in the adsorption process of blue, red, and black wood dyes by AC_{ZnCl₂-850} as shown in Fig. 12.

The positively charged surface of AC_{ZnCl₂-850} when pH is below the pH_{PZC} may promote the electrostatic interaction between activated carbon and dye anions. In addition, the interaction of nitrogen atoms of the adsorbate with free hydrogen atoms of the adsorbent creates H-bonding interactions which contribute to dye adsorption. In the case of the red dye, the different behaviors at 25 mg L⁻¹ as previously mentioned in section 3.3.3 suggest that Lewis acid-base, π - π bond, or hydrophobic effects could also occur. Moreover, the kinetic analysis showed an adsorption process by chemisorption and intraparticle diffusion into the adsorbent pores. This is corroborated by BET and SEM analysis which confirmed the porous structure of the activated carbon that according to the size of the dye molecules may potentially be occupied by them.

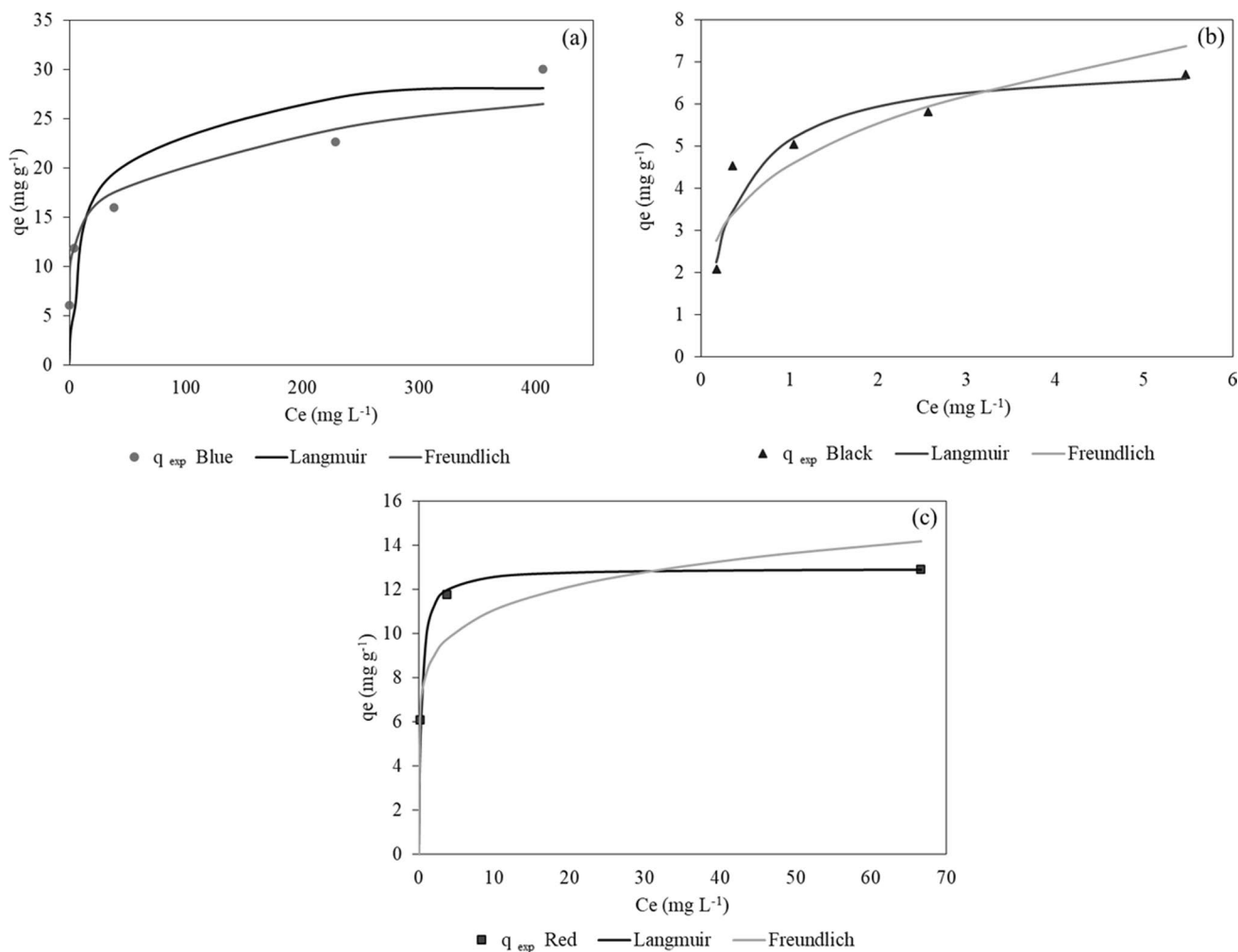


Fig. 11 Experimental and calculated adsorption isotherms of (a) blue, (b) black, and (c) red dyes onto AC_{ZnCl₂-850} (25–500 mg L⁻¹ for blue and black dyes, 25–100 mg L⁻¹ for red dye; pH = 2; adsorbent

dose: 4 g L⁻¹ for blue and red and 2 g L⁻¹ for black; contact time: 48 h for blue and red and 12 h for black dye; temperature: 25°C; agitation speed: 210 rpm)

Table 7 Parameters of the isotherm models for the adsorption of the blue, black, and red dyes on AC_{ZnCl₂-850}

Isotherms	Parameters	Blue dye	Black dye	Red dye
Langmuir	q_m (mg g ⁻¹)	29.4	68.5	13.0
	K_L (L mg ⁻¹)	0.051	0.0134	3.271
	R_L	0.441–0.038	0.749–0.130	0.012–0.0006
	R^2	0.970	0.799	1.000
Freundlich	n	5.71	3.83	7.68
	K_F (mg g ⁻¹ (L mg ⁻¹) ^{-1/n})	9.25	9.85	8.20
	R^2	0.981	0.839	0.839

4 Conclusions

This study has demonstrated that a newly activated carbon with a reasonably good surface area can be prepared

by carbonization and chemical activation of pine (*Pinus radiata*) sawdust with ZnCl₂ as activating agent.

Adsorption of blue, red, and black wood dyes onto activated carbon has been carried out and the adsorption efficiency was remarkably influenced by the variables studied such as adsorbent dose, pH, and initial dye concentration. The results showed that activated carbon had a great adsorption capacity at low dye initial concentration; however, limitations appeared as the concentration increased. Hence, according to the results obtained, AC_{ZnCl₂-850} showed the greatest efficiency of 100% and 96.0% for the blue and red dyes, respectively, at an initial dye concentration of 5 mg L⁻¹, an adsorbent dose of 0.5 g L⁻¹ and natural pH, and only of 55.6% for the black dye at pH = 2 in this case. The complete dye removal was attained at 25 mg L⁻¹ and pH = 2 by increasing the adsorbent dose to 4 g L⁻¹ for blue and red dyes and 2 g L⁻¹ for the black one.

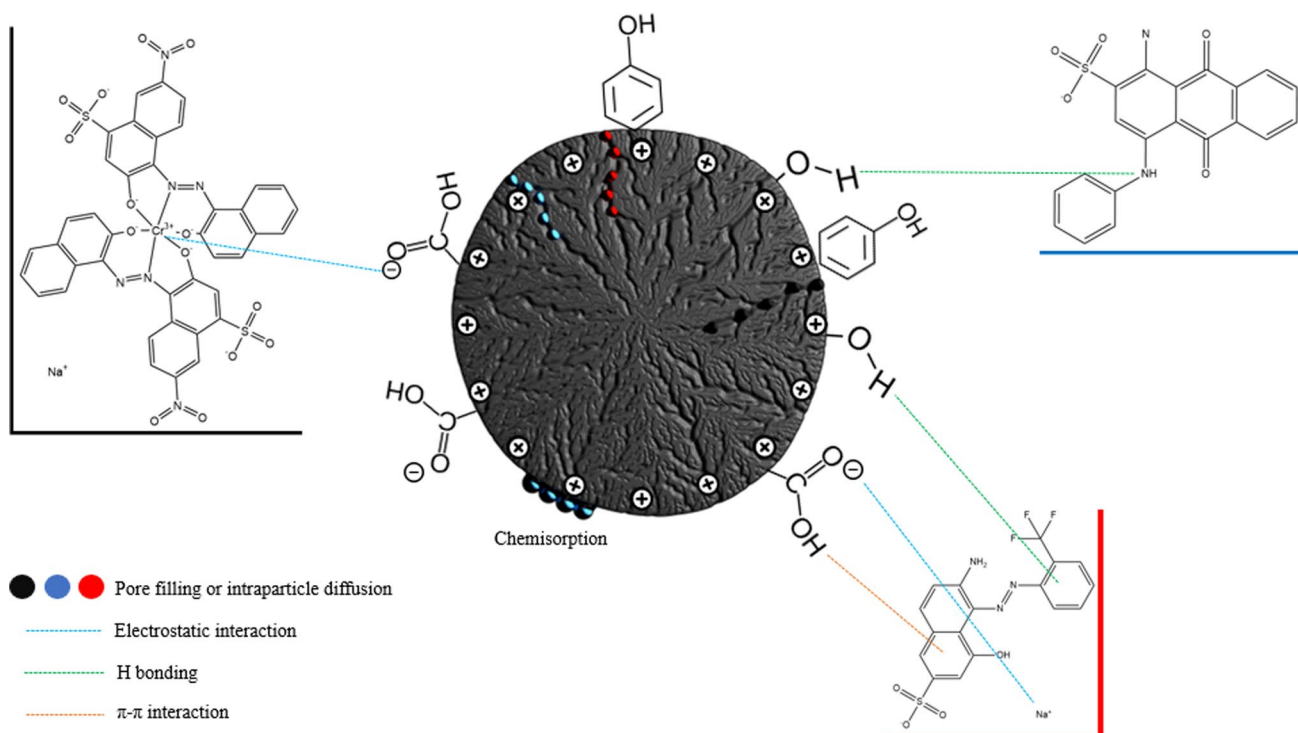


Fig. 12 Proposed adsorption mechanism of blue, red, and black wood dyes on AC_{ZnCl_2-850}

The pseudo-second-order kinetic model was the most appropriate model to describe the removal of wood dyes by the activated carbon prepared and it was demonstrated that intraparticle diffusion was also involved in the adsorption mechanism. Equilibrium data was explained by the Freundlich model for the blue and black dyes and by the Langmuir model for the red dye. Furthermore, dye adsorption by the activated carbon is controlled by several mechanisms including electrostatic forces, H-bonding, pore filling, and π - π interactions.

The present work revealed that the activated carbon prepared from pine sawdust (AC_{ZnCl_2-850}), an abundant and low-cost organic waste, is a promising adsorbent for the removal of dyes from aqueous solutions. The use of biomass based activated carbons instead of the high-cost commercial ones can contribute to the valorization of low-cost renewable wastes and to environmental sustainability goals, offering a green approach for the removal of wood dyes. Further studies must be performed to explore the effect of coexisting contaminants on dye removal.

Supplementary Information The online version contains supplementary material available at <https://doi.org/10.1007/s13399-023-04138-4>.

Authors' contribution Catarina H. Pimentel: investigation, validation, visualization, writing — original draft. M. Sonia Freire: conceptualization, methodology, supervision, funding acquisition, writing — review

and editing. Diego Gómez-Díaz: conceptualization, methodology, supervision, funding acquisition, writing — review and editing. Julia González-Álvarez: conceptualization, methodology, supervision, funding acquisition, writing — review and editing.

Funding Open Access funding provided thanks to the CRUE-CSIC agreement with Springer Nature. This work was supported by Consellería de Educación, Universidade e Formación Profesional, Xunta de Galicia, grant number ED431B 2020/039.

Data availability All data generated or analyzed during this study are included in this article.

Declarations

Ethical approval Not applicable.

Consent for publication All authors agreed to submit this research work for publication.

Competing interests The authors declare no competing interests.

Open Access This article is licensed under a Creative Commons Attribution 4.0 International License, which permits use, sharing, adaptation, distribution and reproduction in any medium or format, as long as you give appropriate credit to the original author(s) and the source, provide a link to the Creative Commons licence, and indicate if changes were made. The images or other third party material in this article are included in the article's Creative Commons licence, unless indicated otherwise in a credit line to the material. If material is not included in the article's Creative Commons licence and your intended use is not

permitted by statutory regulation or exceeds the permitted use, you will need to obtain permission directly from the copyright holder. To view a copy of this licence, visit <http://creativecommons.org/licenses/by/4.0/>.

References

- Jawad AH, Waheeb AS, Rashid RA, Nawawi WI, Yousif E (2018) Equilibrium isotherms, kinetics, and thermodynamics studies of methylene blue adsorption on pomegranate (*Punica granatum*) peels as a natural low-cost biosorbent. *Desalination and Water Treatment* 105:322–331. <https://doi.org/10.5004/dwt.2018.22021>
- Jawad AH, Kadhum AM, Ngoh YS (2018) Applicability of dragon fruit (*Hylocereus polyrhizus*) peels as low-cost biosorbent for adsorption of methylene blue from aqueous solution: kinetics, equilibrium and thermodynamics studies. *Desalination and Water Treatment* 109:231–240. <https://doi.org/10.5004/dwt.2018.21976>
- Bo L, Gao F, Bian Y, Liu Z, Dai Y (2021) A novel adsorbent *Auricularia Auricular* for the removal of methylene blue from aqueous solution: Isotherm and kinetics studies. *Environ Technol Innov* 23:101576. <https://doi.org/10.1016/j.eti.2021.101576>
- Agarwal S, Tyagi I, Gupta VK, Ghasemi N, Shahivand M, Ghasemi M (2016) Kinetics, equilibrium studies and thermodynamics of methylene blue adsorption on Ephedra strobilacea saw dust and modified using phosphoric acid and zinc chloride. *J Mol Liq* 218:208–218. <https://doi.org/10.1016/j.molliq.2016.02.073>
- Piriya RS, Jayabalakrishnan RM, Maheswari M, Boomiraj K, Oumabady S (2021) Coconut shell derived ZnCl₂ activated carbon for malachite green dye removal. *Water Sci Technol* 83(5):1167–1182. <https://doi.org/10.2166/wst.2021.050>
- Chikri R, Elhadiri N, Benchanaa M, El Maguana Y (2020) Efficiency of sawdust as low-cost adsorbent for dyes removal. *J Chem* 2020:1–17. <https://doi.org/10.1155/2020/8813420>
- Yahya MA, Al-Qodah Z, Ngah CWZ (2015) Agricultural bio-waste materials as potential sustainable precursors used for activated carbon production: a review. *Renew Sustain Energy Rev* 46:218–235. <https://doi.org/10.1016/j.rser.2015.02.051>
- Jawad AH, Hum N, Farhan AM, Mastuli MS (2020) Biosorption of methylene blue dye by rice (*Oryza sativa L.*) straw: adsorption and mechanism study. *Desalination and Water Treatment* 190:322–330. <https://doi.org/10.5004/dwt.2020.25644>
- Ahmed MB, Hasan Johir MA, Zhou JL, Ngo HH, Nghiem LD, Richardson C, Moni MA, Bryant MR (2019) Activated carbon preparation from biomass feedstock: clean production and carbon dioxide adsorption. *J Clean Prod* 225:405–413. <https://doi.org/10.1016/j.jclepro.2019.03.342>
- Danish M, Ahmad T (2018) A review on utilization of wood biomass as a sustainable precursor for activated carbon production and application. *Renew Sustain Energy Rev* 87:1–21. <https://doi.org/10.1016/j.rser.2018.02.003>
- Heidarinejad Z, Dehghani MH, Heidari M, Javedan G, Ali I, Sil-lanpää M (2020) Methods for preparation and activation of activated carbon: a review. *Environ Chem Lett* 18(2):393–415. <https://doi.org/10.1007/s10311-019-00955-0>
- Eleri OE, Azuatalam KU, Minde MW, Trindade AM, Muthuswamy N, Lou F, Yu Z (2020) Towards high-energy-density supercapacitors via less-defects activated carbon from sawdust. *Electrochim Acta* 362:137152. <https://doi.org/10.1016/j.electacta.2020.137152>
- González-García P (2018) Activated carbon from lignocellulosics precursors: a review of the synthesis methods, characterization techniques and applications. *Renew Sustain Energy Rev* 82:1393–1414. <https://doi.org/10.1016/j.rser.2017.04.117>
- Ozdemir I, Şahin M, Orhan R, Erdem M (2014) Preparation and characterization of activated carbon from grape stalk by zinc chloride activation. *Fuel Process Technol* 125:200–206. <https://doi.org/10.1016/j.fuproc.2014.04.002>
- Akçakal Ö, Şahin M, Erdem M (2019) Synthesis and characterization of high-quality activated carbons from hard-shelled agricultural wastes mixture by zinc chloride activation. *Chem Eng Commun* 206(7):888–897. <https://doi.org/10.1080/00986445.2018.1534231>
- Hanafi NAM, Abdulhameed AS, Jawad AH, ALOthman ZA, Yousef TA, Al Duaij OK, Alsaari NS (2022) Optimized removal process and tailored adsorption mechanism of crystal violet and methylene blue dyes by activated carbon derived from mixed orange peel and watermelon rind using microwave-induced ZnCl₂ activation. *Biomass Convers Biorefin*:1–13. <https://doi.org/10.1007/s13399-022-03646-z>
- Suhaimi A, Abdulhameed AS, Jawad AH, Yousef TA, Al Duaij OK, ALOthman ZA, Wilson LD (2022) Production of large surface area activated carbon from a mixture of carrot juice pulp and pomegranate peel using microwave radiation-assisted ZnCl₂ activation: an optimized removal process and tailored adsorption mechanism of crystal violet dye. *Diam Relat Mater* 130:109456. <https://doi.org/10.1016/j.diamond.2022.109456>
- Yang Y, Cannon FS (2021) Preparation of activated carbon from pine sawdust with hydrothermal-pressure preconditioning. *J Environ Chem Eng* 9(6):106391. <https://doi.org/10.1016/j.jece.2021.106391>
- Mohanty K, Das D, Biswas MN (2006) Preparation and characterization of activated carbons from *Sterculia alata* nutshell by chemical activation with zinc chloride to remove phenol from wastewater. *Adsorption* 12(2):119–132. <https://doi.org/10.1007/s10450-006-0374-2>
- Wang J, Lei S, Liang L (2020) Preparation of porous activated carbon from semi-coke by high temperature activation with KOH for the high-efficiency adsorption of aqueous tetracycline. *Applied Surface Science* 530:147187. <https://doi.org/10.1016/j.apsusc.2020.147187>
- Kaya N, Yildiz Uzun Z (2020) Investigation of effectiveness of pyrolysis products on removal of alizarin yellow GG from aqueous solution: a comparative study with commercial activated carbon. *Water Sci Technol* 81(6):1191–1208. <https://doi.org/10.2166/wst.2020.213>
- Lopez FA, Centeno TA, Garcia-Diaz I, Alguacil FJ (2013) Textural and fuel characteristics of the chars produced by the pyrolysis of waste wood, and the properties of activated carbons prepared from them. *J Anal Appl Pyrolysis* 104:551–558. <https://doi.org/10.1016/j.jaap.2013.05.014>
- Yumak T (2021) Surface characteristics and electrochemical properties of activated carbon obtained from different parts of Pinus pinaster. *Colloids Surf A: Physicochem Eng Asp* 625:126982. <https://doi.org/10.1016/j.colsurfa.2021.126982>
- Alam S, Khan MS, Bibi W, Zekker I, Burlakovs J, Ghangrekar MM, Bhowmick GD, Kallistova A, Pimenov N, Zahoor M (2021) Preparation of activated carbon from the wood of *Paulownia tomentosa* as an efficient adsorbent for the removal of acid red 4 and methylene blue present in wastewater. *Water* 13(11):1453. <https://doi.org/10.3390/w13111453>
- Cretescu I, Lupascu T, Buciscanu I, Balau-Mindru T, Soreanu G (2017) Low-cost sorbents for the removal of acid dyes from aqueous solutions. *Process Saf Environ Prot* 108:57–66. <https://doi.org/10.1016/j.psep.2016.05.016>
- Heibati B, Rodriguez-Couto S, Al-Ghouti MA, Asif M, Tyagi I, Agarwal S, Gupta VK (2015) Kinetics and thermodynamics of enhanced adsorption of the dye AR 18 using activated carbons prepared from walnut and poplar woods. *Journal of Molecular Liquids* 208:99–105. <https://doi.org/10.1016/j.molliq.2015.03.057>
- Hadi M, Samarghandi MR, McKay G (2010) Equilibrium two-parameter isotherms of acid dyes sorption by activated carbons:

- study of residual errors. *J Chem Eng* 160(2):408–416. <https://doi.org/10.1016/j.cej.2010.03.016>
28. Sarıcı Özdemiç Ç (2019) Equilibrium, kinetic, diffusion and thermodynamic applications for dye adsorption with pine cone. *Sep Sci Technol* 54(18):3046–3054. <https://doi.org/10.1080/01496395.2019.1565769>
 29. Oğana FN, Corral-Rivas S, Gorgoso-Varela JJ (2020) Nonlinear mixed-effect height-diameter model for *Pinus pinaster* ait. and *Pinus radiata* d. Don. *Cerne* 26:150–161. <https://doi.org/10.1590/01047760202026012695>
 30. Zou W, Bai H, Gao S, Li K (2013) Characterization of modified sawdust, kinetic and equilibrium study about methylene blue adsorption in batch mode. *Korean J Chem Eng* 30:111–122. <https://doi.org/10.1007/s11814-012-0096-y>
 31. Carabineiro SAC, Thavorn-Amornsri T, Pereira MFR, Serp P, Figueiredo JL (2012) Comparison between activated carbon, carbon xerogel and carbon nanotubes for the adsorption of the antibiotic ciprofloxacin. *Catal Today* 186(1):29–34. <https://doi.org/10.1016/j.cattod.2011.08.020>
 32. Ho YS, McKay G (1999) Pseudo-second order model for sorption processes. *Process Biochem* 34:451–465
 33. Yakout SM, Hassan MR, El-Zaidy ME, Shair OH, Salih AM (2019) Kinetic study of methyl orange adsorption on activated carbon derived from pine (*Pinus strobus*) sawdust. *BioResources* 14(2):4560–4574. <https://doi.org/10.15376/biores.14.2.4560-4574>
 34. Weber WJ Jr, Morris JC (1963) Kinetics of adsorption on carbon from solution. *Journal of the Sanitary Engineering Division* 89(2):31–59. <https://doi.org/10.1061/JSEDAI.0000430>
 35. Saygılı H, Güzel F (2016) High surface area mesoporous activated carbon from tomato processing solid waste by zinc chloride activation: process optimization, characterization and dyes adsorption. *J Clean Prod* 113:995–1004. <https://doi.org/10.1016/j.jclepro.2015.12.055>
 36. Üner O, Geçgel Ü, Bayrak Y (2019) Preparation and characterization of mesoporous activated carbons from waste watermelon rind by using the chemical activation method with zinc chloride. *Arab J Chem* 12(8):3621–3627. <https://doi.org/10.1016/j.arabj.2015.12.004>
 37. Spagnoli AA, Giannakoudakis DA, Bashkova S (2017) Adsorption of methylene blue on cashew nut shell based carbons activated with zinc chloride: the role of surface and structural parameters. *J Mol Liq* 229:465–471. <https://doi.org/10.1016/j.molliq.2016.12.106>
 38. Thommes M, Kaneko K, Neimark AV, Olivier JP, Rodriguez-Reinoso F, Rouquerol J, Sing KSW (2015) Physisorption of gases, with special reference to the evaluation of surface area and pore size distribution (IUPAC Technical Report). *Pure Appl Chem* 87(9–10):1051–1069. <https://doi.org/10.1515/pac-2014-1117>
 39. Sethia G, Sayari A (2015) Comprehensive study of ultra-microporous nitrogen-doped activated carbon for CO₂ capture. *Carbon* 93:68–80. <https://doi.org/10.1016/j.carbon.2015.05.017>
 40. Balsamo M, Silvestre-Albero A, Silvestre-Albero J, Erto A, Rodriguez-Reinoso F, Lancia A (2014) Assessment of CO₂ adsorption capacity on activated carbons by a combination of batch and dynamic tests. *Langmuir* 30(20):5840–5848. <https://doi.org/10.1021/la500780h>
 41. Açıkyıldız M, Gürses A, Karaca S (2014) Preparation and characterization of activated carbon from plant wastes with chemical activation. *Microporous and Mesoporous Mater* 198:45–49. <https://doi.org/10.1016/j.micromeso.2014.07.018>
 42. Húmpola P, Odetti H, Moreno-Piraján JC, Giraldo L (2016) Activated carbons obtained from agro-industrial waste: textural analysis and adsorption environmental pollutants. *Adsorption* 22(1):23–31. <https://doi.org/10.1007/s10450-015-9728-y>
 43. Domínguez-Ramos L, Prieto-Estalrich A, Malucelli G, Gómez-Díaz D, Freire MS, Lazzari M, González-Álvarez J (2022) N- and S-doped carbons derived from polyacrylonitrile for gases separation. *Sustainability* 14(7):3760. <https://doi.org/10.3390/su14073760>
 44. Akmil-Başar C, Önal Y, Kiliçer T, Eren D (2005) Adsorptions of high concentration malachite green by two activated carbons having different porous structures. *J Hazard Mater* 127(1–3):73–80. <https://doi.org/10.1016/j.jhazmat.2005.06.025>
 45. Ngakou C, Ngomo H, Anagho S (2018) Batch equilibrium and effects of ionic strength on kinetic study of adsorption of phenacetin from aqueous solution using activated carbon derived from a mixture of ayous sawdust and cucurbitaceae peelings. *Curr J Appl Sci Technol* 26(2):1–24. <https://doi.org/10.9734/cjast/2018/37300>
 46. Hock PE, Zaini MAA (2022) Zinc chloride-activated glycerine pitch distillate for methylene blue removal—isortherm, kinetics and thermodynamics. *Biomass Convers Biorefin* 12(7):2715–2726. <https://doi.org/10.1007/s13399-020-00828-5>
 47. Kah M, Sigmund G, Xiao F, Hofmann T (2017) Sorption of ionizable and ionic organic compounds to biochar, activated carbon and other carbonaceous materials. *Water Res* 124:673–692. <https://doi.org/10.1016/j.watres.2017.07.070>
 48. Foroutan R, Peighambari SJ, Peighambari SH, Pateiro M, Lorenzo JM (2021) Adsorption of crystal violet dye using activated carbon of lemon wood and activated carbon/Fe₃O₄ magnetic nanocomposite from aqueous solutions: a kinetic, equilibrium and thermodynamic study. *Molecules* 26(8):2241. <https://doi.org/10.3390/molecules26082241>
 49. Bangash FK, Alam S (2009) Adsorption of acid blue 1 on activated carbon produced from the wood of *Ailanthus altissima*. *Braz J Chem Eng* 26:275–285. <https://doi.org/10.1590/S0104-66322009000200005>
 50. Malarvizhi R, Ho YS (2010) The influence of pH and the structure of the dye molecules on adsorption isotherm modeling using activated carbon. *Desalination* 264(1–2):97–101. <https://doi.org/10.1016/j.desal.2010.07.010>
 51. Shokoohi R, Vatanpoor V, Zarrabi M, Vatani A (2010) Adsorption of Acid Red 18 (AR18) by activated carbon from poplar wood—a kinetic and equilibrium study. *J Chem* 7(1):65–72. <https://doi.org/10.1155/2010/958073>
 52. Bhadusha N, Ananthabaskaran T (2011) Adsorptive removal of methylene blue onto ZnCl₂ activated carbon from wood apple outer shell: kinetics and equilibrium studies. *J Chem* 8:1696–1707. <https://doi.org/10.1155/2011/429831>
 53. Danish M, Hashim R, Ibrahim MM, Sulaiman O (2013) Characterization of physically activated acacia mangium wood-based carbon for the removal of methyl orange dye. *BioResources* 8(3):4323–4339
 54. Hajati S, Ghaedi M, Yaghoobi S (2015) Local, cheap and non-toxic activated carbon as efficient adsorbent for the simultaneous removal of cadmium ions and malachite green: optimization by surface response methodology. *J Ind Eng Chem* 21:760–767. <https://doi.org/10.1016/j.jiec.2014.04.009>
 55. Ghaedi M, Nasab AG, Khodadoust S, Rajabi M, Azizian S (2014) Application of activated carbon as adsorbents for efficient removal of methylene blue: kinetics and equilibrium study. *J Ind Eng Chem* 20(4):2317–2324. <https://doi.org/10.1016/j.jiec.2013.10.007>
 56. Lou K, Rajapaksha AU, Ok YS, Chang SX (2016) Pyrolysis temperature and steam activation effects on sorption of phosphate on pine sawdust biochars in aqueous solutions. *Chem Speciat Bioavailab* 28(1–4):42–50. <https://doi.org/10.1080/09542299.2016.1165080>
 57. Sun D, Zhang Z, Wang M, Wu Y (2013) Adsorption of reactive dyes on activated carbon developed from *Enteromorpha prolifera*. *Am J Anal Chem* 04(07):17–26. <https://doi.org/10.4236/ajac.2013.47a003>
 58. Achour Y, Bahsis L, Ablouh EH, Yazid H, Laamari MR, MEL H (2021) Insight into adsorption mechanism of Congo red dye

onto Bombax Buonopozense bark activated-carbon using central composite design and DFT studies. *Surf Interfaces* 23:100977. <https://doi.org/10.1016/j.surfin.2021.100977>

59. Zhao H, Zhong H, Jiang Y, Li H, Tang P, Li D, Feng Y (2022) Porous ZnCl₂-activated carbon from shaddock peel: methylene blue adsorption behavior. *Materials* 15(3):895. <https://doi.org/10.3390/ma15030895>

Publisher's note Springer Nature remains neutral with regard to jurisdictional claims in published maps and institutional affiliations.